Trans. Phenom. Nano Micro Scales, 7(1): 28-36, Winter and Spring 2019
DOI: 10.22111/tpnms.2018.25600.1157

ORIGINAL RESEARCH PAPER

Implementation of lattice Boltzmann method to study mixing reduction in isothermal electroosmotic pump with hydrophobic walls

Ahmad Reza Rahmati, Hossien Khorasanizadeh, Mohammad Reza Arabyarmohammadi*

Department of Mechanical Engineering, University of Kashan, Kashan 87317-51167, Iran

Received 11June 2018; accepted 11November 2018; available online 30 January 2019

ABSTRACT: The aim of the present work is to analyze the accuracy and to extend the capability of lattice Boltzmann method in slip EOF; a phenomenon which was previously studied by molecular dynamics and less considered by LBM. At the present work, a numerical experiment on boundary conditions of slip velocity is performed and the proportionality of slip with shear stress in electroosmotic pump is proved. Results show that LBM can capture the slip length in EOF with liquid operating fluid. Implementing slip velocity at the walls of a microchannel, the electroosmotic flow with adverse pressure gradient over a hydrophobic surface is investigated in view of mixing reduction. The fluid flow is assumed to be laminar, steady and viscous. Slip at the channel boundaries will decelerate the development process of the flow. Unlike no-slip condition, transverse change in velocity magnitude near the walls decreases and also more resistant pressure is required to create reverse centerline velocity; so mixing probability and performance of EOF pump can alter considerably.

KEYWORDS: *electroosmotic flow; lattice Boltzmann; slip velocity boundary conditions*

INTRODUCTION

Electroosmosis is the electrokinetic way to move the fluids [1]. In electroosmosis, an insulated charged solid placed in contact with the ionized liquid can cause the oppositely charged ions in the liquid gather in front of the solid surface and create a double layer of charges. This phenomenon, exhibited in Figure 1, can be induced by usage of materials like glass or by applying a voltage between a conductive surface and the liquid. Charged layers that arise in liquid can move with an external electric field.

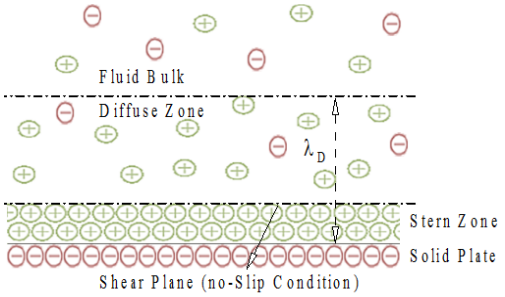

Fig. 1. Schematic view of charge distribution and electric double layer, formed in front of the glass wall [1]

Lattice Bolzmann application in electroosmotic flow has made progress in two last decades.A D2Q9 discretized form of lattice Boltzmann method was applied by Li and Kwok [2] for hydrodynamic analysis of electrolyte solution in microchannels.

*Corresponding Author Email: *ar_rahmati@kashanu.ac.ir*
Tel.: +989132073487; Note. This manuscript was submitted on June 11, 2018; approved on November 11, 2018; published online January 30, 2019.

Tian et al. [3] used lattice Boltzmann for channels with a width of 50 to 800 nm and studied the effects of electrolyte concentration, surface potential, Electric Double Layer (EDL) thickness and the external electric field. Guo et al. [4] coupled finite difference and lattice Boltzmann for electroosmotic flow in microfluidic devices. Study on mixing enhancement in electroosmotic flows was conducted by Wang et al. [5]. Tang et al. [6] implemented lattice Boltzmann method to study the electroosmotic flow with constant and pulsating forces. Using lattice Boltzmann method in electroosmotic flows, Wang et al. [7] demonstrated that there are an ion concentration and optimum width for which the flow rate reaches a maximum. Chai et al. [8] utilized the lattice Boltzmann method to study viscous dissipation of electroosmotic flow in a microchannel. Chai and Shi [9] introduced a new model of lattice Boltzmann equation for Poisson-Boltzmann. Wang et al. [10] used second-order Dirichlet and Neumann boundary conditions in order to highly improve the accuracy of classic methods for solving non-linear Poisson-Boltzmann equation. Application of lattice Boltzmann method to analyze mixing in a cavity of micro-scale has been done by De [11]. Tang et al. [12] added wall blocks and heterogeneous surfaces on the solid boundaries to enhance mixing. Heterogeneous distribution of the surface potential and the phase angle variation of pulsating drive force were the two parameters to produce a vortex which were used by Lin and Chen [13]. In electrokinetic flows, bounce-back modified method was presented by Chen et al. [14].

Nomenclature

b(m)	Numerically Computer Slip Length
c_i(m/s)	Particle Discrete Velocity Vector
c_s(m/s)	Sound Speed
e(Coulomb)	Electron Charge
E(Volt/m)	Strength of External Electric Field
f_i	Density Distribution Function
f_i^{eq}	Density Equilibrium Distribution Function
H(m)	Channel Width
K(Siemens/m)	Electrical Conductivity
K_B(J/°K)	Boltzmann Constant
ℓ (m)	Input Slip Length
L(m)	Channel Length
m	Lattice nodes Across the Channel Width
n_∞(mol/L)	Ion concentration
p(Pascal)	Pressure
p_i	Electric Potential Distribution Function
p_i^{eq}	Electric Potential Equilibrium Distribution Fun
r	Probability factor
r	Position Vector
S	Slip Factor
T_0(°K)	Reference Temperature
V(Volt)	Pumping Potential (Surface Potential)
z	Ionic Species Valance in the Symmetric Solution

Greek Symbols

α	Ionic Energy Parameter
ε(Farads/m)	Electrical Permeability
λ_D(m)	Debye Length
λ_p	Relaxation Time(Poisson-Boltzmann)
λ_u	Relaxation Time (Navier-Stokes)
μ(Pascal.s)	Dynamic Viscosity
ρ(kg/m3)	Density
ρ_{el}(Coulomb/m3)	Charge Density
ξ(Volt)	Zeta Potential
φ(Volt)	Electric Potential
ω_i	Weight Factors

Non-dimensional parameters

E	Unit vector along electric strength
P	$[pH]/[\mu u_{eof}]$
Re	$[\rho_0 u_s H]/\mu(T_0)$
S	ℓ/H
u_{EOF}	$\varepsilon\varepsilon E\xi/\mu$
U	u/u_{EOF}
α	$[ez\xi]/[k_B T_0]$
β	γ^2/α
γ	H/λ_D
Φ_e	φ/ξ
τ	tu_{EOF}/H
$\partial/\partial R$	$\partial/(\partial rH)$

Slip velocity and temperature jump in electroosmotic microchannels are interesting issues.

The slip effects of water flow in hydrophilic and hydrophobic microchannels of 1 and 2mm depth are examined experimentally by Choi et al. [15]. Joseph and Tabeling [16] measured slip velocity in water flowing through thin microchannels, using particle image velocimetry and nanopositioning system. A review of experimental studies by Neto et al. [17] about boundary slippage in Newtonian liquids is presented.

Harting et al. [18] modeled the interaction between hydrophobic channel walls and a fluid by means of a multi-phase lattice Boltzmann model.

Their mesoscopic approach overcomes the limitations of MD simulations and can reach the small flow velocities of known experiments. Slip effects were studied by Ngoma and Erchiqui [19], in a pressure driven electroosmotic microchannel. Slip over hydrophobic walls is numerically studied by Eijkel [20]. primary studies suggest that in electroosmotic flows, the first layer of liquid molecules is not in motion and the particles start to move past the shear plane corresponding to negative slip length in Navier boundary condition.

The slip length can be positive in electroosmotic flows and therefore, electroosmotic velocity equation is modified, as in equation 1 [20]; which expresses the slip is proportional to the velocity gradient at the wall, as schematically illustrated in Figure 2.

$$u_{slip\ EOF} = -\frac{\varepsilon\xi E}{\mu}\left(1+\frac{b}{\lambda_D}\right)\frac{V}{\xi} \quad (1)$$

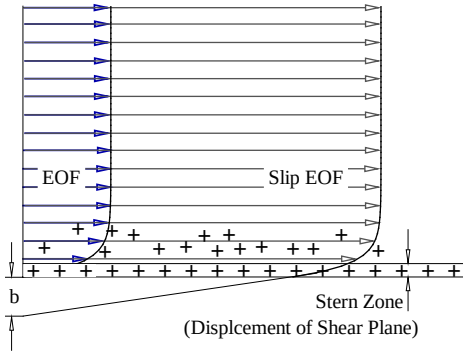

Fig. 2. Slip electroosmotic flow over the microchannel wall [24]

Surface wettability due to surface charge can reduce the slip length [21]. According to the molecular dynamics simulation of non-wetting charged surfaces, Joly et al. [22] found that 40 times the Helmholtz-Smoluchowski velocity may be reached before the slip charactristic is reduced. Tandon and Kirby [23] studied electrokinetic phenomena on hydrophobic polymers such as Teflon and Zeonor. Using Nerst-Planck Navier-Stokes equations, De et al. [24] studied nanochannel walls covered with super hydrophobic materials. A sequence of slip and non-slip boundary conditions in pairs next to each other was defined on thechannel walls. Sadeghi et al. [25] have studied

electroosmotic flow in a hydrophobic micro duct with Debye–Hückel approximation. The slip characteristic of microchannel walls due to solid-liquid interaction via LBM is still being studied. Navier boundary condition is the first and most widely used method for calculating the slip velocity of fluids over solid walls. In gases, the Knudsen number (dimensionless mean free path) is used as the coefficient of differentiated velocity at the wall that has a clear physical meaning. But for liquids which are the working fluid of the present work, this factor will be different according to the interaction coefficient of solid-fluid and creates constant slip length. The second method uses a potential function of interaction that is added to the collision function. This function has an exponential behavior, which represents exponential decrease in density near the wall and works similar to hyperbolic function of electroosmotic force. The potential function of Interaction has constant factor that is calculated based on the interaction of wall with the fluid and results in constant slip length. This method has been applied by Benzi et al. [26], Yan et al. [27] and Zhu et al. [28].

The last method is the use of combined boundary condition of bounce-back and reflection that has a probability factor which is similar to previous ones and determines the amount of slip length.

It is part of LBM that has been validated experimentally by Tretheway et al. [21]. Rahmati and Niazi [29] have taken advantage of it for microcavities. It should be noted that Diffuse Scattering Boundary Condition (DSBC) can also show slip velocity at the walls; but because of independency to the wall properties, it cannot be considered as a general method. In general, it can be concluded that all three methods express one concept; the velocity derivative factor in the first method, or solid-liquid interaction coefficient in the second one, or the probability factor in the third method is equivalent to a specified slip and actual slip velocity cannot be calculated merely by numerical methods and without these three factors. Only in the first method, the slip length can be defined directly as a problem input, and then the results should be checked to see if the slip velocity represents the specified slip length. So this method is used in the present work. The electroosmotic force,which is equivalent to the potential function of interaction, also shows that a combination of the first and second method is utilized in the present work. According to the conducted literature survey, slip velocity at the walls of an electroosmotic microchannel have not been considered well by LBM. In the present work, an attempt has been made to extend the application of lattice Boltzmann method by implementing slip velocity at the walls of a microchannel to study the electroosmotic flow behaviour with inclusion of hydrophobic surface and adverse pressure gradient.

PROBLEM DEFINITION

In the present work, flow in a microchannel with hydrophobic surfaces affected by electroosmotic force and adverse pressure gradient is studied. The velocity distribution within channel is investigated. The liquid is water and the flow is assumed to be laminar, steady and viscous. There is an analogy between slip factor in liquids and Knudsen number in gas flows and that's why a slip factor of 0.08 has been applied as the coefficient of wall velocity derivative in boundary conditions. The simulations are carried out with a 10^{-8}(s) time step in a channel width of 20 μm and aspect ratio of 40 while Reynolds number is 1.0. According to values of $\alpha = \frac{[ez\xi]}{[k_B T_0]}$ and $\beta = \frac{\gamma^2}{\alpha}$ which are equal to 0.01 and 1.6×10^5 respectively, ion concentration will be $3.43 \times 10^{-7}(mol/L)$. Electroosmotic parameters are chosen according to study of Shi et al. [30].

In the present work, a grid structure of 100×4000 in 2-D geometry is employed and as presented in Figure 3. EDL has been chosen small enough in order to prevent overlap.

This study is carried out, followed that of Shi et al. [30], by lattice Boltzmann method with discrete model of D2Q9 and applying slip at the hydrophobic walls of an electroosmotic pump to simulate the fluid behavior.

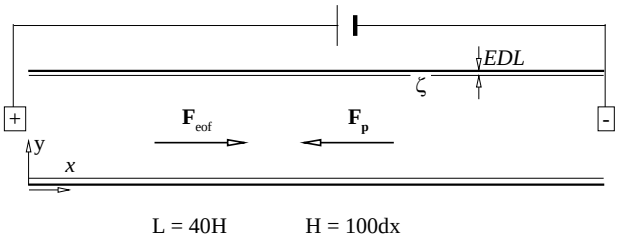

Fig. 3. Schematic of the problem model of a two-dimensional microchannel between two plates

GOVERNING EQUATIONS

Mathematically, the electric potential distribution and fluid flow in electroosmos is phenomenon can be explained by a combination of Poisson-Boltzmann and Navier-Stokes equations. The Navier-Stokes equation for electroosmotic flow has a volumetric force that involves electro-kinetic effect. The volumetric force depends on the charge density which is obtained by Poisson-Boltzmann equation.

In this non-linear system, these equations must be solved simultaneously. At the present work, a D2Q9 Lattice Boltzmann model introduced by Guo *et al.* [4] for electroosmotic flows is utilized to solve the governing equations (equation 2 and equation 3).

Discrete Lattice Boltzmann Model for Electroosmotic Flow

To extract the lattice Boltzmann model, at first, two discrete two-dimensional equations with BGK linear approximation are presented in equations 2 and 3for Poisson-Boltzmann and Navier-Stokes equations [30].

$$\frac{\partial p_i}{\partial \tau} + c_i \cdot \frac{\partial}{\partial R} p_i = -\frac{1}{\lambda_p}\left(p_i - p_i^{eq}\right) + Q_i \qquad (2)$$

$$\frac{\partial f_i}{\partial \tau} + c_i \cdot \frac{\partial}{\partial R} f_i = -\frac{1}{\lambda_u}\left(f_i - f_i^{eq}\right) + F_i \quad (3)$$

Where $\varepsilon = \lambda_p c_s^2 / D_e$ and $\mu / Re = \rho c_s^2 \lambda_u$. p_i and f_i are the distribution functions of electric potential and density fields. For each function, a discretized form in space and time, separated into two parts of collision and propagation, can be exhibited. This form that was conducted for f_i has been shown in equations 4 and 5 [31]. λ_p, and λ_u, as functions of fluid and flow properties, represent the relaxation times and c_is are the discrete velocities.

Local collision:

$$f_i(x,t) = \frac{1}{\lambda_u} f_i^{eq} + (1 - \frac{1}{\lambda_u}) f_i(x,t) \quad (4)$$

Non local propagation:

$$f_i(x + \boldsymbol{c_i}\Delta t, t + \Delta t) = f_i(x,t) \quad (5)$$

Local equilibrium distribution functions are defined in equations 6 and 7 by p_i^{eq}, and f_i^{eq} [30] are:

$$p_i^{eq} = \omega_i \Phi_e \quad (6)$$

$$f_i^{eq} = \omega_i \rho \left[1 + \frac{c_i \cdot U}{c_s^2} + \frac{(c_i \cdot U)^2}{2c_s^4} - \frac{U^2}{2c_s^2}\right] \quad (7)$$

Where in $\omega_0 = 4/9$, $\omega_{1,2,3,4} = 1/9$ and $\omega_{5,6,7,8} = \frac{1}{36}$[30]. Q_i represents the electric charge density (ρ_{el}) that is expressed dimensionless in equation 8, [30].

$$Q_i = D_e \omega_i \beta \, sinh(\alpha \Phi_e) \quad (8)$$

D_e is the parameter to set the value of λ_p in equation 2 [30]. F_i is equal to the volume force of electroosmotic and pressure that is defined in equations 9 and 10 [30].

$$F_{i(EOF)} = \frac{\omega_i \beta}{Re} sinh(\alpha \Phi_e) \, E \cdot \left(\frac{c_i - U}{c_s^2} + \frac{c_i \cdot U}{c_s^4} c_i\right) \quad (9)$$

$$F_{i(Pressure)} = \omega_i \frac{\partial p}{\partial x} \frac{c_i}{c_s^2} \quad (10)$$

The macroscopic variables and the values of electric potential, density and velocity are defined in equation (11-13) [30].

$$\Phi_e = \sum_{i=0}^{8} p_i \quad (11)$$

$$\rho U = \sum_{i=0}^{8} f_i c_i \quad (12)$$

$$\rho = \sum_{i=0}^{8} f_i \quad (13)$$

Boundary Conditions

In each of the two governing equations, periodic boundary conditions (equations 14 and 15) are used at the ends of the channel [32]:

$$f_{i_{(in)}} = f_{i_{(out)}} \quad (14)$$

$$p_{i_{(in)}} = p_{i_{(out)}} \quad (15)$$

In electric potential equations, equating condition of aligned non-equilibrium distribution functions is applied as in equation 16 to specify unknown functions at the walls [32]. Non-dimensional electric potential at the walls equals one; representing $\frac{V}{\xi} = 1$. Difference between V and ξ can amplify the slip according to Equation1 which is not considered in the present work.

$$p_i - \omega_i = p_{i+2} - \omega_{i+2}, i = 1,2,5,6 \quad (16)$$

Unknown wall quantities of density function are determined by equations (17-20). A simple algorithm is presented in [33] showing how to use these relations.

$$f_i - f_i^{eq} = f_{i+2} - f_{i+2}^{eq}, i = 1,2,5,6 \quad (17)$$

$$\rho = f_0 + f_1 + f_2 + f_3 + f_4 + f_5 + f_6 + f_7 + f_8 \quad (18)$$

$$\rho u = f_1 - f_3 + f_5 - f_6 - f_7 + f_8 \quad (19)$$

$$\rho v = f_2 - f_4 + f_5 + f_6 - f_7 - f_8 \quad (20)$$

In slip condition, u in equation 19 is calculated by equation 21 [20], being discretized in first-order three-point derivative.

$$u_{x_{fluid\ near\ wall}} = S\frac{\partial u_x}{\partial y} \rightarrow u_{fluid\ near\ wall} = mS\frac{-u_{x_{m-2}} + 4u_{x_{m-1}}}{2 + 3mS} \quad (21)$$

In section 5, a combined boundary condition of bounce-back and reflection in equations (22-24) is also utilized instead of equations (17-20) to capture slip velocity at the walls.

$$f_2 = f_4 \tag{22}$$

$$f_5 = r \times f_7 + (1 - r) \times f_8 \tag{23}$$

$$f_6 = (1 - r) \times f_7 + r \times f_8 \tag{24}$$

RECOVERED MACROSCOPIC EQUATIONS

Charge density and electric potential are linked together via Poisson equation $\varepsilon \nabla^2 \varphi(r) = -\rho_{el}(r)$. The differential of Poisson-Boltzmann [6] equation and its dimensionless form which is recovered from equation 2 are:

$$\varepsilon \nabla^2 \varphi(r) = -2zen_\infty \sinh\left[\frac{ze}{k_B T_0}\varphi(r)\right] \tag{25}$$

$$\frac{\partial}{\partial R} \cdot \left(\varepsilon \frac{\partial \Phi_e}{\partial R}\right) = \beta \sinh(\alpha \Phi_e) \tag{26}$$

For a charged solid boundary, changes are only normal to the microchannel walls. The wall boundary condition for Poisson-Boltzmann equation states that $\varphi(0) = \xi$. Debye length, estimates electric double layer thickness with great precision [6] as:

$$\lambda_D = \sqrt{\frac{\varepsilon k_B T_0}{2z^2 e^2 n_\infty}} \tag{27}$$

When an external electric field is applied between the two channel ends, the electroosmotic force is applied to the electric double layer of ions and the surrounding fluid is drawn with. The fluid volume is transferred by viscosity. Velocity profile across the channel grows in the small time interval between the moments of the potential being applied and the electroosmotic flow being fully developed. Steady state profile flattens and the velocity across the channel width remains constant, except for the electric double layer. Given that Navier-Stokes equation is linear in the low Reynolds; the overall profile of flow, in presence of reverse pressure, is obtained by superposition of pressure and electroosmotic flow ($u_{total} = u_{EOF} - u_P$). For both flows, the maximum velocity occurs in the channel center. Movement in the electrolyte solution can be modeled by the incompressible mass and Navier-Stokes equations with the electroosmotic volumetric force in equation 28 and equation 29 [30].

These dimensionless relations are the macroscopic equations governing the electroosmotic flow in microchannels which are recovered from equations 3.

$$\frac{\partial}{\partial R} \cdot U = 0 \tag{28}$$

$$\frac{\partial U}{\partial \tau} + U.\frac{\partial}{\partial R}U = -\frac{1}{Re}\frac{\partial}{\partial R}P + \frac{1}{Re}\frac{\partial}{\partial R} \cdot \left(\mu \frac{\partial}{\partial R}U\right) + \frac{\beta}{Re}\sinh(\alpha \Phi_e)E \tag{29}$$

VERIFICATION AND VALIDATION

Mesh dependency has been done for m quantities of 50, 100 and 200. The difference in u values relates to the near wall region in EDL. The numerical result of velocity distribution that is presented in Figure 4 confirms using m equal to 100.

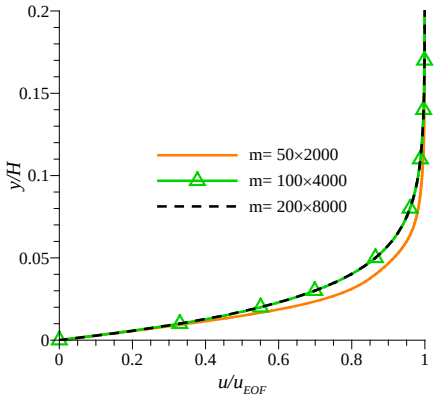

Fig. 4. Velocity distribution across the EOF microchannel with three mesh structures

In computing, the convergence criterion, equation 30 is defined as the number of iterations and the least square root of the squares summations of the velocity field components in the channel.

$$\sqrt{\sum_{j=0}^{m}\sum_{i=0}^{n}\frac{(u_{x_{t+\Delta t}} - u_{x_t})_{i,j}^2 + (u_{y_{t+\Delta t}} - u_{y_t})_{i,j}^2}{mn}} < 1 \times 10^{-7}. \tag{30}$$

Analytical equations presented by Guo et al. [4] are used for numerical algorithm validation. Figure 5 exhibits the accuracy of the method and the results obtained.

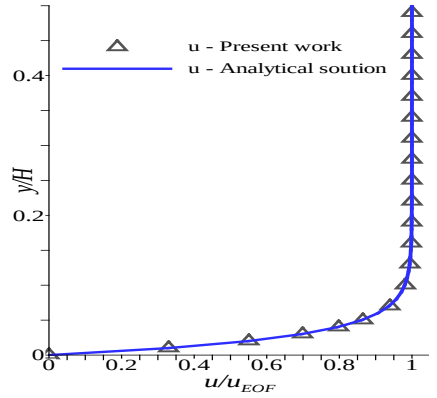

Fig. 5. Velocity distribution across the EOF microchannel with constant physical property

According to the assumptions utilized to extract equations (31-33) [4], validation results with the present work inputs that are defined in section 2 will be compared in no-slip and constant physical property mode.

$$\varphi = \frac{cosh\left(\gamma\left(\frac{y}{H} - 0.5\right)\right)}{cosh(\gamma/2.0)} \tag{31}$$

$$u_{EOF} = 1.0 - \varphi + \sum_{n=1}^{\infty} A_n \, sin\left(n\pi \frac{y}{H}\right) exp\left(-\frac{n^2\pi^2 t}{Re}\right) \tag{32}$$

$$u_P = 0.5 \frac{dp}{dx} \frac{y}{H}\left(\frac{y}{H} - 1\right) \tag{33}$$

Where in $A_n = -2a^2\,(1-(-1)^n)/n\pi(n^2\pi^2 + a^2)$. In order to validate the results of the computer program for the slip case with Yang and Liu [34], a microflows under electrosmootic force (exponentially decaying force) is studied using a combined boundary condition of bounce-back and reflection (r=0.85) and also usage of Navier boundary condition (S=0.008). In Figure 6, a 30% slip (velocity at the wall to that of the channel center) could show good agreement for $\gamma = 65$. Other inputs are presented in [34].

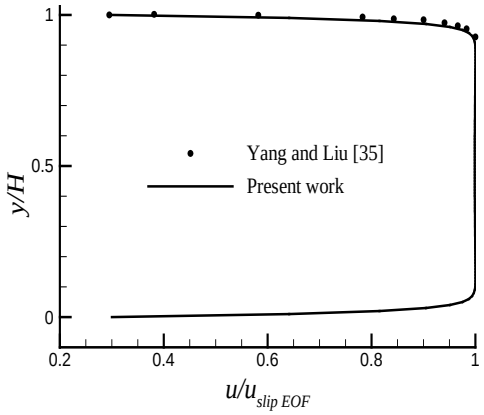

Fig. 6. Velocity profile across the microchannel with γ = 65, r = 0.85, S = 0.008

Tretheway et al. [21] announced that we are unable to determine if the slip velocity is proportional to the shear stress but Figurer 3 showed that usage of Navier boundary condition is a tool to prove this relation over hydrophobic surfaces of an EOF microchannel with liquid as the operating fluid.

For verification studies of hydrophobic channels, the slip length is calculated from the relation presented by Joly et al. [22] $\left[b = \lambda_D\left(\frac{u_{slip}}{u_{no-slip}} - 1\right)\right]$ and is compared to the coefficient of velocity derivatives in numerical calculations [$\ell = S \times H$]; which results in difference between b and ℓ by less than 4%. This proves the accuracy of the relation for the slip velocity.

RESULTS AND DISCUSSION

In what follows, slip velocity is applied at the walls. Time development of velocity profile and changes of electroosmotic flow are presented.

Next, inclusion of adverse pressure force with EOF and the resultant flow behavior are discussed. Finally, increase in Debye length which is an agent for mole concentration is studied.

Applying slip at the solid boundaries of EOF

Slip velocity is applied at the walls of EOF microchannel with constant physical properties. Electroosmotic is the only force to move the fluid and no other external drive exists. Velocity variations and the time evolution of velocity distribution to reach the steady state are studied. Figure 7 shows the effect of slip boundary condition on velocity distribution in an EOF microchannel with constant physical properties that demonstrates an increase in the electroosmotic velocity at the channel center to 4 times and the wall slip velocity reaches 75% of maximum speed.

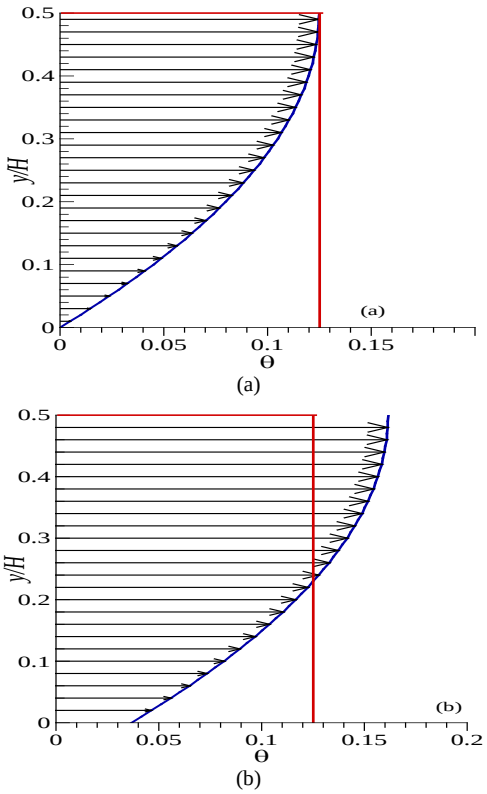

Fig. 7. Velocity distribution across the EOF microchannel the a) without slip effect b) with slip effect

This velocity increase was predicted by July et al. [22] for hydrophobic surfaces. Apart from mathematical point of view, contribution of stern zone to fluid movement can be

the main physical reason for velocity enhancement at the walls which substantially decreases the viscous effects and increases velocity at the channel center.

The dimensionless electroosmotic flow velocity, in terms of developed mode, in a cross section at 6 different time steps is presented in Figure 8.

Comparing the quality of velocity profiles at different times shows that development happens faster, in the case of no-slip condition than the slip mode, at the channel walls and center. By applying an electric field, velocity derivative increases over time at the channel walls and the slip velocity rises. The convergence of the profile, observed in Figure 8, says that steady state has reached faster compared with that of no slip velocity distribution.

For example, at the time of 175 μs, latency equals to 50 μs during the profile formation.

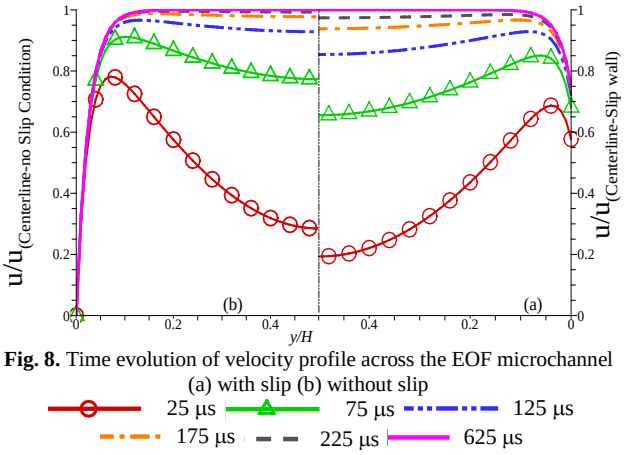

Fig. 8. Time evolution of velocity profile across the EOF microchannel (a) with slip (b) without slip

Applying adverse pressure gradient to slip EOF

Adverse pressure gradient with inclusion of no-slip and no-jump boundary conditions are added to the electroosmotic flow studied in section 6-1. Flow behaviors with the both boundary conditions of slip and no-slip in response to the additional pressure force are investigated. The resultant velocity distributions in the EOF microchannel have been presented in Figure 9 and 10. The numerical simulation is consistent with the conclusion of analytical relation in the no slip condition which indicates a slowdown as much as 0.625m/s (numbered 2 in Fig. 9) at the center of the channel.

The average velocity halves when the pressure gradient acts in the opposite direction of electroosmotic force (numbered 1 in Fig. 9) and brings the profile out from the plug-like state. The maximum velocity is located near the walls.

Given that velocity is not binding on the walls, the pressure can reduce the slip (numbered 3 in Fig. 10) and the whole velocity profile is driven backwards.

As a result, the velocity variation across the channel is less and the ratio of velocity at the channel center to the velocity near the walls drops to a lesser amount.

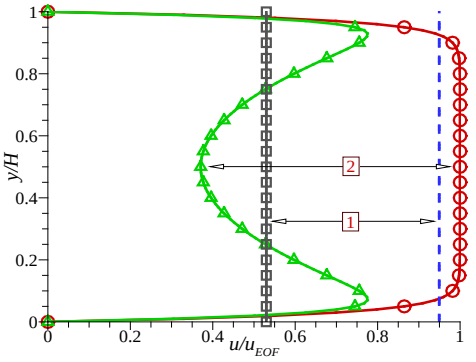

Fig. 9. Velocity distribution across the non-slip EOF microchannel △ with adverse pressure gradient ○ without adverse pressure gradient
Average u (EOF)
Average u (EOF+Adv. Press.)

Percentage of mass flow rate variation for the slip condition due to the pressure is much less than that of the no-slip one (numbered 1 in Fig. 10).

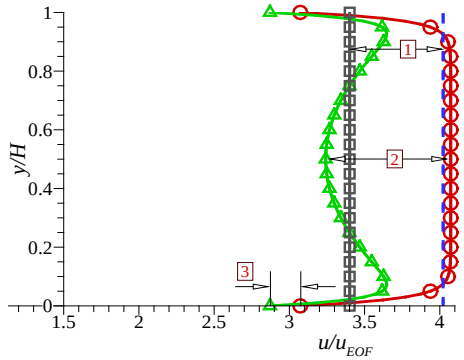

Fig. 10. Velocity distribution across the slip EOF microchannel △ with adverse pressure gradient ○ without adverse pressure gradient
Average u (EOF)
Average u (EOF+Adv. Press.)

Applying resistant pressure force can generate two reverse flows in microchannel if it increases enough. Figure 11 states that slippage at the walls necessitate more required pressure (up to 3 times greater than that of the no-slip condition) to overcome the primary flow.

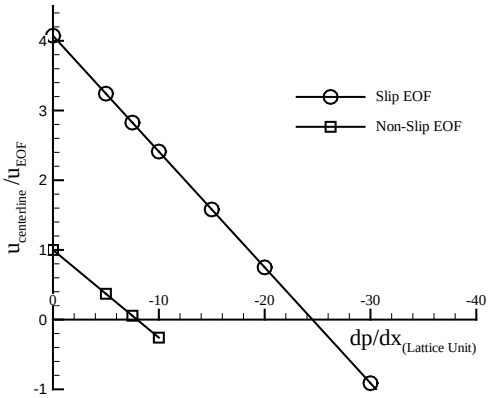

Fig. 11. Centerline velocity variation due to resistant pressure gradient

Debye length effects on electric potential

Although implementation of slip boundary condition with constant Reynolds will change the potential distribution but at the present work it is assumed to have negligible effects due to large values of γ. Figure 12 shows the electric potential across the microchannel, demonstrating more penetration of surface potential into the fluid.

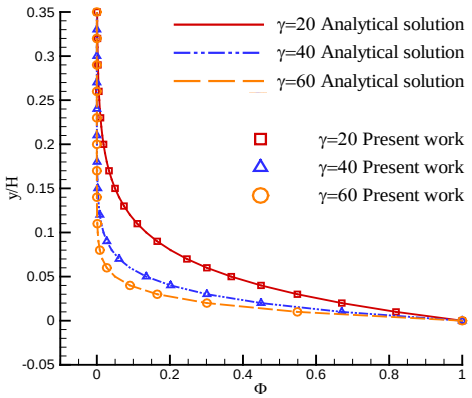

Fig. 12. Eelctric potential distribution across the channel

Analysis of velocity derivate at the boundaries in Figure 13 represents a slight deviation from linear behavior which is a sign of error growth. Because Debye length decreases; so more lattice nodes are required to capture velocity variation in stern and diffuse layers.

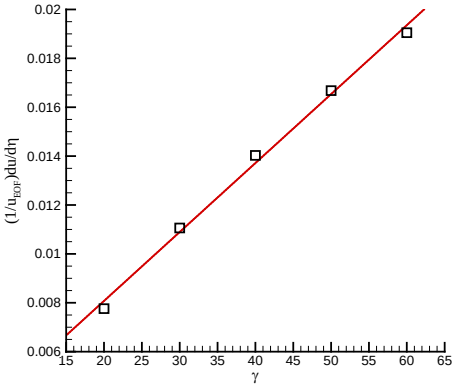

Fig. 13. Changes of wall velocity derivative over γ (□). Expected linear behaviour (⟶)

CONCLUSION

In the present work, an attempt has been made to verify the applicability of lattice Boltzmann method in calculating the slip length in electroosmotic flow over hydrophobic walls. Combination of bounce-back and reflection boundary conditions, potential function of interaction and Navier are three methods commonly used to analyze slip in LBM. The present work validates a discrete model of D2Q9 with Navier boundary condition for investigation of Slip EOF, which was formerly performed by MD. The results show that slip at the channel boundaries will increase the development time of flow which is not an advantage because of reduced slip length due to surface charge. However, slip on the walls while preventing transverse changes in velocity profiles, causes a significant increase from quantity point of view which improves the performance of EOF pump. The accuracy of relations being used to calculate the velocity of the channel walls is acceptable, according to conducted verification between b and ℓ.

Unlike no slip manner at presence of reverse direction force, hydrophobic channels bear less variation in magnitude at the channel cross section and mixing capability falls down greatly. The velocity magnitude at the boundaries and centerline are of the same order, so they are not an accounted choice for mixers. At the channel center where pressure drive is the dominant force, reverse velocity increases and at the near wall region, where the EOF is the key force, flow velocity grows considerably, especially for the slip case.

It is suggested to extend this work for compressible fluids with pressure boundary condition. On the other hand, a microchannel of overlapped electric double layers is an interesting and applicable field for hydrophobic surfaces of EOF micropumps, which can be analysed by lattice Boltzmann method.

REFERENCES

[1] Hamad MA, Ferdows M. Similarity solutions to viscous flow and heat transfer of nanofluid over nonlinearly stretching sheet. Applied Mathematics and Mechanics. 2012 Jul 1;33(7):923-30.

[2] Choi SU, Zhang ZG, Yu W, Lock wood FE, Grulke EA. Anomalous thermal conductivity enhancement in nanotube suspensions. Applied physics letters. 2001 Oct 1;79(14):2252-4.

[3] Aminossadati SM, Ghasemi B. Natural convection cooling of a localised heat source at the bottom of a nanofluid-filled enclosure. European Journal of Mechanics-B/Fluids. 2009 Oct 31;28(5):630-40.

[4] Xie H, Lee H, Youn W, Choi M. Nanofluids containing multiwalled carbon nanotubes and their enhanced thermal conductivities. Journal of Applied physics. 2003 Oct 15;94(8):4967-71.

[5] Chol SU. Enhancing thermal conductivity of fluids with nanoparticles. ASME-Publications-Fed. 1995 Nov 12;231:99-106.

[6] Abu-Nada E, Chamkha AJ. Mixed convection flow in a lid-driven inclined square enclosure filled with a nanofluid. European Journal of Mechanics-B/Fluids. 2010 Dec 31;29(6):472-82.

[7] Sheikhzadeh GA, Arefmanesh A, Kheirkhah MH, Abdollahi R. Natural convection of Cu–water nanofluid in a cavity with partially active side walls. European Journal of Mechanics-B/Fluids. 2011 Apr 30;30(2):166-76.

[8] Hassan H. Heat transfer of Cu–water nanofluid in an enclosure with a heat sink and discrete heat source. European Journal of Mechanics-B/Fluids. 2014 Jun 30;45:72-83.

[9] Bourantas GC, Skouras ED, Loukopoulos VC, Burganos VN. Heat transfer and natural convection of nanofluids in porous media. European Journal of Mechanics-B/Fluids. 2014 Feb 28;43:45-56.

[10] Rana P, Bhargava R. Flow and heat transfer of a nanofluid over a nonlinearly stretching sheet: a numerical study. Communications in Nonlinear Science and Numerical Simulation. 2012 Jan 31;17(1):212-26.

[11] De A K. Numerical Modeling of Microscale Mixing Using Lattice Boltzmann Method. Ph.D. thesis. Virginia Polytechnic Institute and State University, Blacksburg, Virginia, 2008.

[12] Tang GH, Li XF, Tao WQ. Microannular electro-osmotic flow with the axisymmetric lattice Boltzmann method. Journal of Applied Physics. 2010 Dec 1;108(11):114903.

[13] Lin T Y, Chen C L. Analysis of electroosmotic flow with periodic electric and pressure fields via the lattice Poisson–Boltzmann method. Applied Mathematical Modelling. 2013:37(5):2816-2829.

[14] Chen Q, Zhou H, Jiang X, Xu L, Li Q, Ru Y. Extension of the Improved Bounce-Back Scheme for Electrokinetic Flow in the Lattice Boltzmann Method. Entropy. 2015:17(11):7406-7419.

[15] Choi CH, Westin KJ, Breuer KS. Apparent slip flows in hydrophilic and hydrophobic microchannels. Physics of fluids. 2003 Oct;15(10):2897-902.

[16] Joseph P, Tabeling P. Direct measurement of the apparent slip length. Physical Review E. 2005 Mar 31;71(3):035303.

[17] Neto C, Evans DR, Bonaccurso E, Butt HJ, Craig VS. Boundary slip in Newtonian liquids: a review of experimental studies. Reports on Progress in Physics. 2005 Oct 10;68(12):2859.

[18] Harting J, Kunert C, Herrmann HJ. Lattice Boltzmann simulations of apparent slip in hydrophobic microchannels. EPL (Europhysics Letters). 2006 Jun 23;75(2):328.

[19] Ngoma GD, Erchiqui F. Heat flux and slip effects on liquid flow in a microchannel. International Journal of Thermal Sciences. 2007 Nov 1;46(11):1076-83.

[20] Eijkel J C T. Liquid slip in micro-and nanofluidics: recent research and its possible implications. Lab Chip. 2007;7(3):299-301.

[21] Tretheway D C, Zhu L, Petzold L, Meinhart C. Examination of the slip boundary condition by μ-PIV and lattice Boltzmann simulations. in: ASME 2002 International Mechanical Engineering Congress and Exposition. New Orleans. Louisiana. USA. 2002:551-556.

[22] Joly L, Ybert C, Trizac E, Bocquet L. Liquid friction on charged surfaces: From hydrodynamic slippage to electrokinetics. The Journal of chemical physics. 2006 Nov 28;125(20):204716.

[23] Tandon V, Bhagavatula SK, Nelson WC, Kirby BJ. Zeta potential and electroosmotic mobility in microfluidic devices fabricated from hydrophobic polymers: 1. The origins of charge. Electrophoresis. 2008 Mar;29(5):1092-101.

[24] De S, Bhattacharyya S, Hardt S. Electroosmotic flow in a slit nanochannel with superhydrophobic walls. Microfluidics and Nanofluidics. 2015 Dec 1;19(6):1465-76.

[25] Sadeghi M, Sadeghi A, Saidi MH. Electroosmotic flow in hydrophobic microchannels of general cross section. Journal of Fluids Engineering. 2016 Mar 1;138(3):031104.

[26] Benzi R, Biferale L, Sbragaglia M, Succi S, Toschi F. Mesoscopic two-phase model for describing apparent slip in micro-channel flows. EPL (Europhysics Letters). 2006 Apr 12;74(4):651.

[27] Yan-Yan C, Hou-Hui Y, Hua-Bing L. Boundary slip and surface interaction: a lattice Boltzmann simulation. Chinese Physics Letters. 2008 Jan;25(1):184.

[28] Zhu L, Tretheway D, Petzold L, Meinhart C. Simulation of fluid slip at 3D hydrophobic microchannel walls by the lattice Boltzmann method. Journal of Computational Physics. 2005 Jan 1;202(1):181-95.

[29] Rahmati AR, Niazi S. Application and Comparison of Different Lattice Boltzmann Methods on Non-Uniform Meshes for Simulation of Micro Cavity and Micro Channel Flow. Computational Methods in Engineering. 2015 Jul 15;34(1):97-118.

[30] Shi Y, Zhao TS, Guo ZL. Lattice Boltzmann simulation of thermal electro-osmotic flows in micro/nanochannels. Journal of Computational and Theoretical Nanoscience. 2008 Feb 1;5(2):236-46.

[31] Mohamad A A. Lattice Boltzmann method: fundamentals and engineering applications with computer codes: Springer Science & Business Media. 2011.

[32] Zou Q, He X. On pressure and velocity boundary conditions for the lattice Boltzmann BGK model. Physics of Fluids. 1997:9(6):1591-1598.

[33] Rahmati A R, Khorasanizadeh H, Arabyarmohammadi M R. Application of Lattice Boltzmann Method for Simulating MGD in a Microchannel under Magnetic Field Effects. Modares Mechanical Engineering. 2016:16 (7):229-240.

[34] Yang D, Liu Y. Numerical simulation of electroosmotic flow in hydrophobic microchannels. Science in China Series E: Technological Sciences. 2009 Aug 1;52(8):2460-5.